Terrestrial, Atmospheric
and Oceanic Sciences

ORIGINAL ARTICLE   **Open Access**

Multifractal measures of the 2021 earthquake swarm in Hualien, Taiwan

Jeen-Hwa Wang[1,2*], Kou-Cheng Chen[1], Kou-Chang Chen[3] and Kwang-Hee Kim[4]

Abstract

An earthquake swarm occurred in Haulien, Taiwan, from April 7 to August 31, 2021. The epicenters are in the range from 23°47′ N to 24°04′ N and from 121°25′ E to 121°42′ E. $C_q(r)$ and $C_q(t)$ are the generalized correlation integral of r and t, respectively. From the events with local magnitudes ≥ 3 and focal depths ≤ 25 km, $C_q(r)$ is calculated for the epicentral and hypocentral distribution (using the distance between two events, r) and $C_q(t)$ for the time sequence (using the inter-event time between two events, t). The multifractal dimension D_q (q = 2, 3, …, 15) is the slope of the linear portion of the log–log plots of $C_q(r)$ versus r as well as $C_q(t)$ versus t. For the epicentral distribution, the linear pattern is in the range $0.5 \leq \log(r) \leq 1.3$. The measured values of D_q are all smaller than 2 that is the spatial dimension and monotonically decreases with increasing q. This indicates that the epicentral distribution of the swarm is multifractal. For the hypocentral distribution, a lack of a wide enough linear pattern on the log–log plot makes the hypocentral distribution be not multifractal. For the time sequence, the log–log plot of $C_q(t)$ versus t shows a linear pattern in the range $0.5 \leq \log(t) \leq 1.0$. The values of D_q are all smaller than 1 that is the time dimension and monotonically decreases with increasing q, thus suggesting multifractality of the time sequence when t is shorter than the maximum inter-event time.

Keywords: Epicentral and hypocentral distributions, Time sequence, Multifractal dimension

1 Introduction

The Philippine Sea plate moves northwestward with a speed of about 8 cm/year (Yu et al. 1997) to collide the Eurasian plate in Taiwan (e.g., Hsu 1971; Tsai et al. 1977; Wu 1978). The collision boundary is almost along the eastern coastal line of Taiwan. The collision yields high seismicity in the region (Hsu 1961; Wang et al. 1983; Wang 1988a, 1998; Wang and Shin 1998). The Hualien area is located around the northern segment of the collision boundary. Historically, many large earthquake sequences, for example, the 1951 sequence (e.g., Chen et al. 2007; Lee et al. 2008), the 1986 sequence (Chen and Wang 1986, 1988; Liaw et al. 1986; Wang, 1988b, 1998; Yeh et al. 1990), the 2002 sequence (e.g., Chen et al. 2004),

and the 2018 sequence (e.g., Hwang et al. 2018; Kou-Chen et al. 2018; Wu et al. 2019), occurred in the area. The 1951 earthquake sequence and the 2018 earthquake caused serious damage in the area. Hence, the studies of earthquakes in the area are important and significant for both scientific interest and social needs.

The Central Weather Bureau reported the occurrence of an earthquake swarm with the largest event of local magnitude $M_L = 6.2$ in Hualien, Taiwan, during April 7–August 31, 2021. The events are located at an area from 23°47′ N to 24°04′ N and from 121°25′ E to 121°42′ E. The focal depths, H, of the events were mainly in the range 0–25 km. Since an earthquake swarm does not often happen in the area, it is significant to investigate its characteristics.

There are numerous scaling laws, for example, the frequency-magnitude law (Gutenberg and Richter 1944), scaling laws of earthquake faults (see Wang 2018), and scaling law of earthquake source spectra (see Wang

*Correspondence: jhwang@earth.sinica.edu.tw
[1] Institute of Earth Sciences, Academia Sinica, Nangang, P.O. Box 1-55, Taipei, Taiwan
Full list of author information is available at the end of the article

2019), to describe self-similarity or scale-invariance of earthquakes and faults. In 1950's, a mathematician Benoit B. Mandelbrot proposed the concept of fractal geometry with fractal dimension to describe the self-similar or scale-invariant natural phenomena (see Mandelbrot 1983). His concept has deeply influenced the Euclidean geometry. Mandelbrot (1989) measured fractal dimensions for geophysical problems. Fractal geometry has been widely applied to describe earthquake phenomena, including the spatial distributions of earthquakes (e.g., Hirata 1989; Turcotte 1989; Hirabayashi et al. 1992; Wang and Lin 1993; Wang and Lee 1995, 1996; Wang and Shen 1999; Wang et al. 2014; Fan and Lin 2017; Sri Lakshmi and Banerjee 2019; Hui et al. 2020), the time sequences of earthquakes (e.g., Smalley et al. 1987; Hirata 1989; Kagan and Jackson 1991; Ogata and Abe, 1991; Papadopoulos and Dedousis 1992; Koyama et al. 1995; Wang 1996; Wang and Lee 1995; Tang et al. 2012; Wang et al. 2014; Hui et al. 2020), the fault activities (e.g., Aviles et al. 1987; Okubo and Aki 1987; Lee 1995; Chang et al. 2007; Zhao et al. 2011; Ni et al. 2017), and the preseismic electromagnetic (EM) signals (e.g., Gotoh et al. 2003; Kiyashchenko et al. 2004; Ida et al. 2012; Smirnova et al. 2012). The studies made by Tang et al. (2012), Hui et al. (2020), Gotoh et al. (2003), Kiyashchenko et al. (2004), Ida et al. (2012), and Smirnova et al. (2012) are concerning the preseismic seismicity and EM signals for predicting an impending earthquake. These studies are useful for the estimates of seismic hazard.

For a fractal set of objects, the Hausdorff–Besicovitch dimension is not exactly equal to the Euclidean or topological dimension (Mandelbrot 1983). Mandelbrot (1983) defined the fractal dimension to represent a fractal set. Since the Hausdorff–Besicovitch's definition is not convenient for measuring the fractal dimension of a set of objects in the real world, several different fractal dimensions have been defined (e.g., Grassberger and Procaccia 1983; Takayasu 1990). Four commonly-used dimensions are the similarity dimension D_S, the capacity dimension D_{CA}, the information dimension D_I, and the correlation dimension D_C. Their definitions can see Takayasu (1990). In general, the relationship among the four dimensions is $D_S = D_{CA} \geq D_I \geq D_C$. The equality $D_S = D_{CA} = D_I = D_C$ holds only for homogeneous fractal sets. Most sets of natural objects are not perfectly self-similar and indeed multifractal, thus leading to $D_S = D_{CA} > D_I > D_C$. This indicates that a single fractal dimension is not good enough to characterize the fractal properties of natural objects. Therefore, fractality of objects has been extended from a single fractal dimension to the multifractal (or generalized fractal) dimension, D_q (Grassberger 1983; Hentshe and Procaccia 1983). Wang and Lee (1995) assumed that it is more complete to represent multifractality of a set of
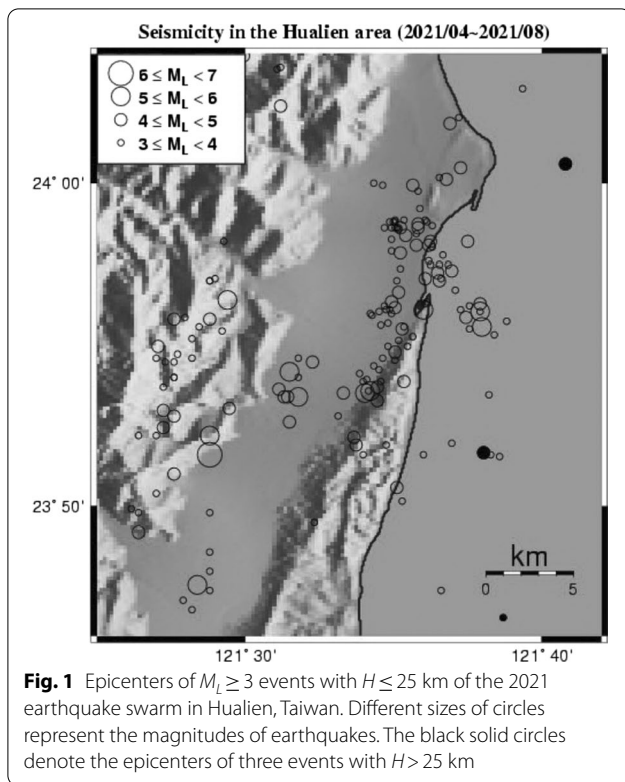
objects by using a D_q–q relation than by only taking the above-mentioned four fractal dimensions.

In this study, we will explore the self-similarity of the 2021 Haulien earthquake swarm by measuring the multifractal dimensions of $M_L \geq 3$ events with $H \leq 25$ km for both the spatial distributions and time sequence. In the space domain, both the epicentral and hypocentral distances are taken into account.

2 Data

Since 1991, the Central Weather Bureau (CWB) has upgraded her old seismic network, by adding many new stations. This new network is named the CWB Seismic Network (CWBSN). In 1992 the Taiwan Telemetered Seismographics Network (TTSN), that was originally operated by the Institute of Earth Sciences, Academia Sinica (Wang 1989), was merged into the CWBSN. The earthquake magnitude of the earthquake catalogue has been unified to be the local magnitude (Shin 1992) that is denoted as M_L. A detailed description about the CWBSN can be found in Shin (1992) and Shin and Chang (2005). The CWBSN is now composed of 72 stations, each equipped with three-component digital velocity seismometers, and many accelerations and broadband seismometers. The seismograms are recorded in both high- and low-gain forms. This network provides high-quality digital earthquake data to the seismological community. The data used in this study are directly retrieved from the CWB data base.

The earthquake epicenters of the swarm are plotted in Fig. 1. The location uncertainty of epicenter is about 2 km and the depth uncertainty is about 5 km (Shin and Chang 2005). The earthquakes with $M_L \leq 6.2$ occurred in an area from 23°47′ N to 24°04′ N and from 121°25′ E to 121°42′ E. We have to consider the size of the study area. The length of one degree of latitude slightly varies with latitude, while that of longitude remarkably varies with latitude (see Karney 2012). The lengths of one degree of latitude and one degree of longitude may be calculated from https://www.nhc.noaa.gov/gccalc.shtml which is the website of the National Hurricane Center, National Oceanic and Atmospheric Administration, USA. For the study area, the average lengths are ~ 31.13 km along the latitude, i.e., the NS direction, and ~ 28.62 km along the longitude, i.e., the EW direction. Hence, the study area is 31.13×28.62 km$^2 = 890.99$ km^2. The figure exhibits that most of the events are located at the Longitudinal Valley, some at the Costal Range, and some offshore. Figure 2a shows the depth distribution of number of events in a 5-km range along a selected longitude. The focal depths of the events were mainly in the range 0–25 km: a few events in the depth range 0–5 km and most of the events in the depth range 5–10 km. Wang et al. (1994) reported

Fig. 1 Epicenters of $M_L \geq 3$ events with $H \leq 25$ km of the 2021 earthquake swarm in Hualien, Taiwan. Different sizes of circles represent the magnitudes of earthquakes. The black solid circles denote the epicenters of three events with $H > 25$ km

that inland earthquakes in Taiwan are located mainly in the depth range 0–12 km and the number of events remarkably decrease with increasing depth. The crust-upper mantle boundary with $v_p = 7.5$ km/s in the Taiwan region is mainly in the range 35–45 km as inferred by several authors (e.g., Rau and Wu 1995; Ma et al. 1996; Kim et al. 2005). Hence, an average depth of 40 km is taken as a boundary to classify the events: a crustal event with $H \leq 40$ km and an upper-mantle or subduction-zone event with $H > 40$ km. Hence, most of the events of the earthquake swarm are crustal earthquakes. Figure 2 also shows that there are three events with $H > 25.0$ km. Their epicenters that are all offshore are displayed by solid circles in Fig. 1.

Figure 2b shows the time sequence of earthquake magnitudes for $M_L \geq 3$ events with $H \leq 25$ km. Clearly, the time sequence is not uniform. The frequency of events is high in some short time intervals and low in others. The largest inter-event time is 8.742 days and the shortest one is smaller than 1 day.

3 Multi-fractal dimension
3.1 Spatial distributions of earthquakes
The multifractal or generalized fractal dimension, D_q, in the space domain is defined by the following expression (Grassberger 1983; Hentschel and Procaccia 1983):

$$D_q = \lim[\log(\Sigma p_i^q)/\log(\delta)]/(q-1) \tag{1}$$

where the parameter q can be any real number in the range from $-\infty$ to ∞ and p_i is the probability that an event falls into a box with a length δ. D_q at large, positive q shows the fractal property of dense regions with large p_i; while D_q at large, negative q displays that of thin regions with small p_i. D_q for negative q may be larger than the spatial (or topological) dimension, d ($d = 2$ for the 2D space and $d = 3$ for 3D space), in Euclidean geometry. There is no geometric sense for $D_q > d$ (Mandelbrot, 1989). For a set of objects, the value of D_q at small q shows the fractal property of its coarse structure and that at large q exhibits the fractal property of its fine structure. For $q \geq 0$, the largest D_q is D_0 and D_q decreases with increasing q. If two sets of objects have the same D_q–q relations, they are considered to be statistically similar. Note that D_0, D_1, and D_2 are equivalent to the capacity dimension D_{CA}, information dimension D_I, and correlation dimension D_C, respectively.

The probability p_i may be estimated by the box-counting method from the observed data. Since such a method requires a large number of data, it is not so useful in practice. Kurths and Herzel (1987) suggested a correlation integral method as described below. A local density function $n_j(r)$ is defined by the following expression:

$$n_j(r) = \Sigma_k Q(r - |\mathbf{r}_j - \mathbf{r}_k|)/(N-1) \tag{2}$$

where the value of $\Theta(s)$ is 1 if $s \geq 0$ and 0 if $s < 0$. In Eq. (2), r_j and r_k are the position vectors of events j and k, respectively, and thus $|r_j - r_k|$ is the distance between the two events. A vector r_i is denoted by $< x_i, y_i, z_i >$ where x_i, y_i, and z_i are the latitude multiplied by 111 km, the longitude multiplied by 111 km, and the focal depth (in km), respectively. The value of 111 km is almost the length of 1° along both latitude and longitude on the ground surface (Oncel et al. 1995). Hence, a generalized correlation integral $C_q(r)$ for the distance between two events is defined by
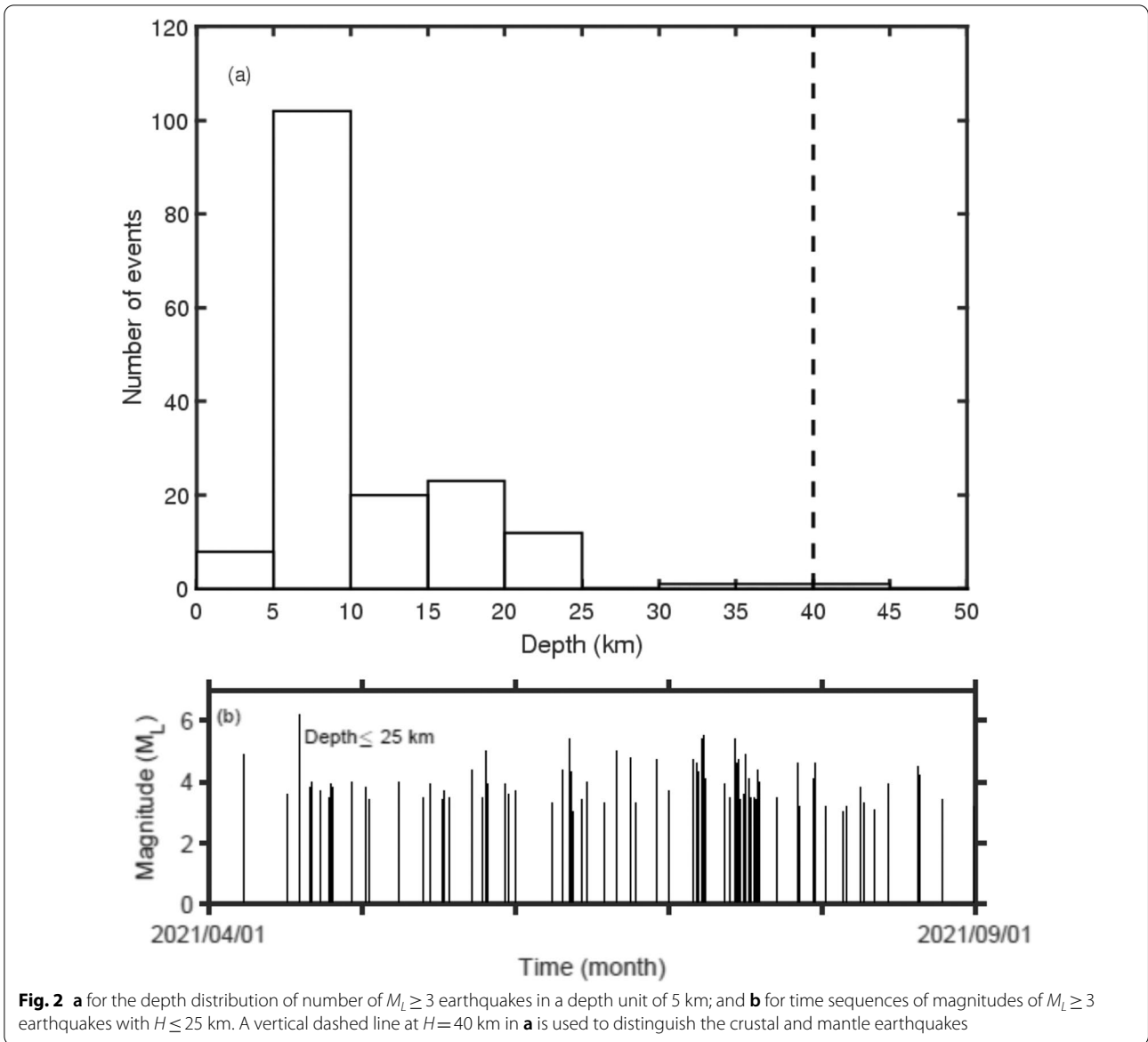
$$C_q(r) = \left[\Sigma n_j^{q-1}(r) \right]^{1/(q-1)}. \tag{3}$$

$C_q(r)$ is considered to be related to r in the following power-law function with the scaling exponent D_q:

$$C_q(r) \sim r^{D_q}. \tag{4}$$

There are two kinds of distance. The first one is the epicentral distance:

$$r_{jk} = |\mathbf{r}_j - \mathbf{r}_k| = \left[(x_j - x_k)^2 + (y_j - y_k)^2 \right]^{1/2}. \tag{5}$$

Fig. 2 **a** for the depth distribution of number of $M_L \geq 3$ earthquakes in a depth unit of 5 km; and **b** for time sequences of magnitudes of $M_L \geq 3$ earthquakes with $H \leq 25$ km. A vertical dashed line at $H = 40$ km in **a** is used to distinguish the crustal and mantle earthquakes

This gives the so-called 2D measure. The second one is the hypocentral distance:

$$r_{jk} = |\mathbf{r}_j - \mathbf{r}_k| = \left[(x_j - x_k)^2 + (y_j - y_k)^2 + (z_j - z_k)^2 \right]^{1/2}. \quad (6)$$

This gives the so-called 3D measure.

When the study area is large, Hirata (1989) considered the spherical effect for r_{jk} from the formula: $r_{jk} = \cos^{-1}[\cos\theta_j \cos\theta_k + \sin\theta_j\sin\theta_k\cos(\phi_j - \phi_k)]$ where θ_i and ϕ_i are, respectively, the co-latitude and longitude of event i on the spherical surface. Some authors (e.g.,Oncel et al. 1995; Telesca et al. 2001; Marquez-Ramirez et al. 2012) used this formula to calculate the distance between two events for large study areas. However, since the area of this study is small (<1°

along both the latitude and the longitude), it is not necessary to consider the spherical effect. Hence, our calculations for r_{jk} are merely based on Eqs. (5) and (6).

3.2 Time sequence of earthquakes

In order to study multifractal behavior of time sequence of earthquakes, Wang and Lee (1995) replaced the two spatial quantities by a time interval t and an inter-event time $|t_i - t_k|$, respectively. Hence, a generalized correlation integral $C_q(t)$ for the time sequence is

$$C_q(t) = \left[\Sigma n_j^{q-1}(t) \right]^{1/(q-1)}. \quad (7)$$

$C_q(t)$ is considered to be related to t in the following power-law function with the scaling exponent D_q:

$$C_q(t) \sim t^{Dq}. \tag{8}$$

In the followings, first the values of $C_q(r)$ and $C_q(t)$ will be calculated from the data. Secondly, the log–log plots of $C_q(r)$ versus r and those of $C_q(t)$ versus t at different q's will be first constructed. Finally, the value of D_q is evaluated from the slope of the linear portion of data points. In this study, only the values of D_q at positive $q = 2, 3, ..., 15,$ are calculated because we are only interested in the fractal properties of denser areas and time intervals.

4 Results

4.1 Spatial distributions of earthquakes
The value of $C_q(r)$ are calculated from the spatial distributions of earthquakes of the 2021 Hualien swarm. The log–log plots of $C_q(r)$ versus r at $q = 2, 3, ..., 15$ are displayed in Fig. 3 for the 2D measure and in Fig. 4 for the 3D measure. In the two figures, the value of q increases from bottom to top. Since the uncertainty of epicenter is 2 km and the uncertainty of focal depth is about 5 km as mentioned above, the smallest distance, r_l, is taken to be the average of the two values, i.e., 3.5 km, thus giving $\log(r_l) = 0.54$. In the following, we take $\log(r_o) = 0.5$. Since the lengths along the EW and along the NS direction are 31.13 km and 28.62 km, respectively, as mentioned above and the deepest focal depth is 25.0 km, the longest distance, r_c, is $(31.13^2 + 28.62^2)^{1/2}$ km $= 42.29$ km for the 2D measure and $(31.13^2 + 28.62^2 + 25.0^2)^{1/2}$ km $= 49.12$ km for the 3D measure. This gives $\log(r_c) = 1.63$ for the 2D measure and $\log(r_c) = 1.69$ for the 3D measure. Li et al. (1994) suggested that the upper bound of the linear portion, r_c, should be 30% or 50% of the largest distance
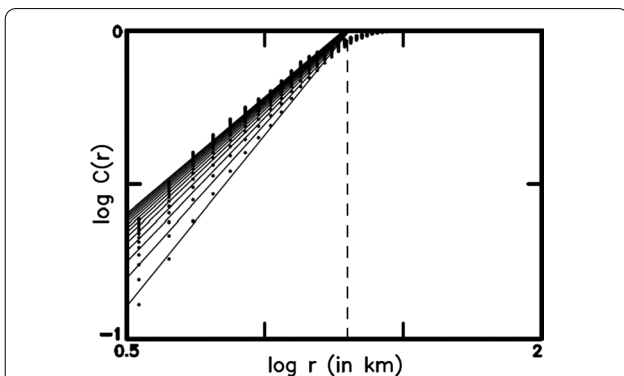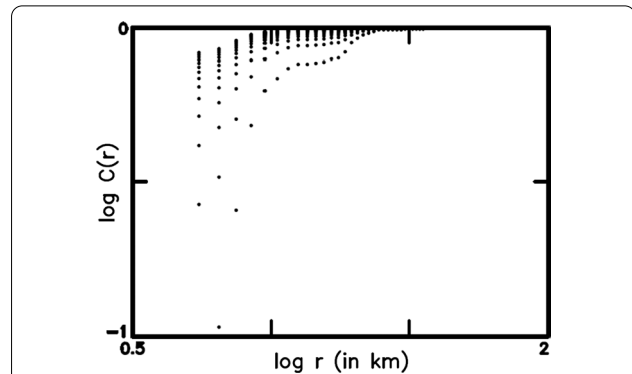

Fig. 4 The log–log plot of $C_q(r)$ versus r at $q = 2, 3, ..., 15$ (from bottom to top) for $M_L \geq 3$ events under 3D measure

between two events to avoid the possible existence of roll-over. According to their criterion, the value of r_c of this study must be shorter than 12.69 km or 21.15 km for the 2D measure and 14.74 km or 24.56 km for the 3D measure. Nevertheless, r_c is here still taken to be 50.7 km, i.e., $\log(50.7) = 1.71$, for both 2D and 3D measures for the purpose of examining the possible existence of 'roll-over' which means that the deflection of data points from the regression line more or less in a shape of part of a circle. Hence, the data points are plotted in the range $0.5 \leq \log(r) \leq 1.71$. The regression line is inferred from the data in the range $0.5 \leq \log(r) \leq 1.3$. In Fig. 3, a vertical dashed line denotes $\log(r_u) = 1.3$. The degree of scattering of data points is higher in Fig. 4 than in Fig. 3.

In Fig. 3 for the 2D measure, the data points are well distributed around a linear trend when $0.5 \leq \log(r) \leq \log(r_u)$ where r_u is the upper bound distance, and the data points are roll-over when $\log(r) > \log(r_u)$. The value of $\log(r_u)$ is 1.5 and thus $r_u = 10^{1.5}$ km $= 31.6$ km, which is 74.72% of $r_c = 42.29$ km, for the 2D measure. The percentage for the 2D measure is 24.72% higher than the upper bound by Li et al. (1994). However, Fig. 5 displays that for 3D measure a linear pattern of log–log plot of $C_q(r)$ versus r at each q, especially at larger q, appears only in a narrow range of $\log(r)$. Hence, we do not measure the values of D_q for the 3D measure. The least-squared method is applied to infer a linear regression equation to fit the linear portion of data points. D_q is just the slope value of the linear equation. For the 2D measure, the values of D_q at $q = 2, 3, ..., 15$ and their standard deviations are listed in Table 1. The obtained D_q–q relations are shown in Fig. 5 with solid circles. Clearly, D_q decreases with increasing q.

4.2 Time sequence of earthquakes
For the multifractal measures in the time domain, the maximum inter-event time is 8.792 days. The generalized correlation integral functions $C_q(t)$ versus inter-event

Fig. 3 The log–log plot of $C_q(r)$ versus r at $q = 2, 3, ..., 15$ (from bottom to top) for $M_L \geq 3$ events under 2D measure. The solid lines represent the regression lines inferred from the data points with $0.5 \leq \log(r) \leq 1.5$. A vertical dotted line denotes the upper bound of $\log(r)$, i.e., $\log(r_u) = 1.3$, for conducting linear regression
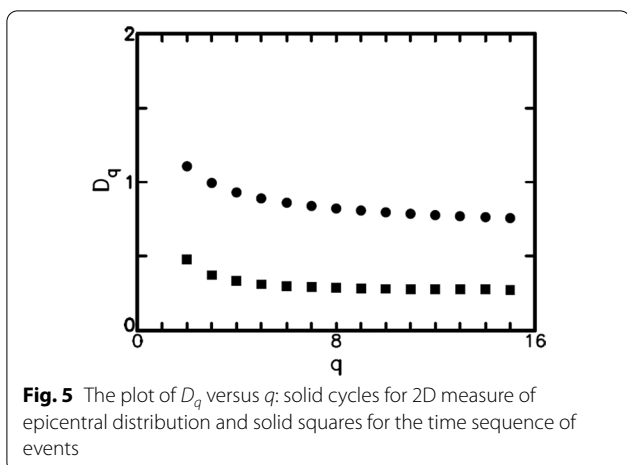
Fig. 5 The plot of D_q versus q: solid cycles for 2D measure of epicentral distribution and solid squares for the time sequence of events
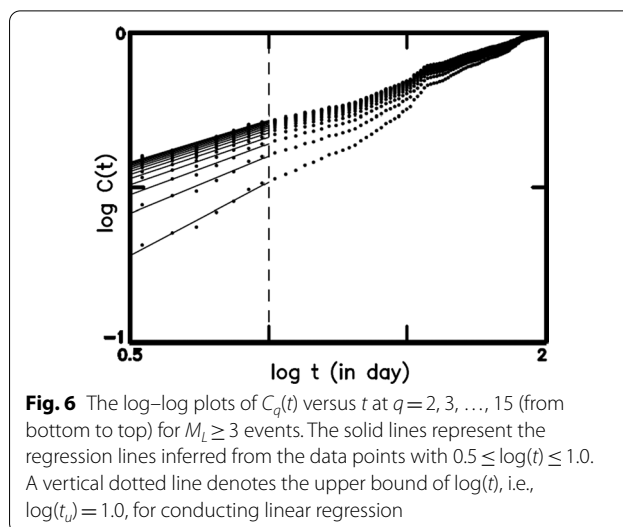

Fig. 6 The log–log plots of $C_q(t)$ versus t at $q = 2, 3, …, 15$ (from bottom to top) for $M_L \geq 3$ events. The solid lines represent the regression lines inferred from the data points with $0.5 \leq \log(t) \leq 1.0$. A vertical dotted line denotes the upper bound of $\log(t)$, i.e., $\log(t_u) = 1.0$, for conducting linear regression

Table 1 The values of D_q with standard errors at $q = 2, 3, …, 15$ for the spatial distribution of events under 2D measure and those for the time sequence of events

q	2D measure $(0.5 \leq \log(r) \leq 1.3)$	Time sequence $(0.5 \leq \log(t) \leq 1.0)$
02	1.107 ± 0.006	0.475 ± 0.014
03	0.995 ± 0.006	0.371 ± 0.012
04	0.933 ± 0.006	0.330 ± 0.011
05	0.890 ± 0.006	0.309 ± 0.010
06	0.861 ± 0.006	0.296 ± 0.010
07	0.839 ± 0.006	0.289 ± 0.009
08	0.822 ± 0.006	0.284 ± 0.009
09	0.808 ± 0.006	0.280 ± 0.009
10	0.777 ± 0.006	0.278 ± 0.009
11	0.786 ± 0.006	0.276 ± 0.009
12	0.777 ± 0.006	0.275 ± 0.009
13	0.770 ± 0.006	0.274 ± 0.009
14	0.763 ± 0.006	0.2733 ± 0.009
15	0.757 ± 0.006	0.272 ± 0.009

time t in days between two events at $q = 2, 3, …, 15$ are calculated from the data. The log–log plot of $C_q(t)$ versus t are displayed in Fig. 6, in which the value of q increases from bottom to top. The data points are plotted in the range $0.5 \leq \log(t) \leq 2.15$. The upper bound time interval is $t_c = 10^{2.15}$ days $= 140$ days that is almost equal to the time period of the swarm, i.e., 139.779 days. Obviously, the data points are linearly well distributed only in a range $0.5 \leq \log(t) \leq \log(t_u)$ where $\log(t_u) = 1.0$ and thus $t_u = 10^{1.0}$ days $= 10$ days. In Fig. 6, a vertical dotted line denotes $\log(t_u) = 1.0$. The regression line is plotted in the range $0.5 \leq \log(t) \leq 1.0$. When $\log(t) > 1.0$, the pattern of data points shows 'roll-over'. Hence, the values of D_q that are evaluated from the data points are listed in Table 1.

The D_q–q relation is shown in Fig. 5 with solid squares. Clearly, D_q decreases with increasing q. From Table 1, the evaluated values of D_q for the two cases are considered to be acceptable because the deviations of D_q at all q's are lower than 0.014.

5 Discussion
5.1 Spatial distributions of earthquakes
For the epicentral distributions of earthquakes, the log–log plots of $C_q(r)$ versus r are displayed in Fig. 3 for the 2D measure. There is a linear pattern when $0.5 \leq \log(r) \leq 1.3$ in Fig. 3. Results clearly suggest that the epicentral distribution of $M_L \geq 3$ events of the Hualien swarm is multifractal. In advance, the linear pattern of data points does not appear in the whole range of $\log(r)$ or r. This means that the finite size effect of the study area might influence multifractality. The finite size effect is also reported by Wang et al. (2014). The value of $\log(r_u)$ of the linear portion is 1.3 or $r_u = \sim 20.0$ km. The lengths along the latitude and longitude are 31.13 km and 28.62 km, respectively. This gives the longest length of the 2D structure to be $r_c = 42.29$ km. Figure 1 shows that the epicenters are distributed almost in the entire study area along the longitude and latitude. Hence, for the 2D measure r_u is shorter than r_c and comparable to the length either along the latitude or along the longitude. Figure 3 also show that the pattern of data points is roll-over when $\log(r) > 1.3$ because the values of $\log[C_q(r)]$ for $\log(r) > 1.3$ are smaller than those calculated from the linear regression equation done from the data points with $0.5 \leq \log(r) \leq 1.3$. Table 1 demonstrates that the values of D_q for the 2D measure have the largest one of 1.107 and much smaller than 2 that is the spatial dimension in Euclidean geometry. This

reflects the existence of many large voids in the 2D space of the study area (see Fig. 1). This makes the multifractal dimensions be much smaller than the space dimension, i.e., $d = 2$.

For the hypocentral distribution of earthquakes, the log–log plots of $C_q(r)$ versus r are displayed in Fig. 4 for the 3D measure. The linear pattern only appears in a narrow range of $\log(r)$. Results clearly suggest that the hypocentral distribution of $M_L \geq 3$ events of the Hualien swarm is not multifractal. The upper bound of $\log(r_u)$ for the linear pattern of data points is ~ 1.0, thus giving $r_u = 10$ km. This reflects the finite size effect of the study area on multifractality. Since the deepest focal depth in use is 25 km, the longest length of the 3D structure is $r_c = 50.7$ km. Nevertheless, Fig. 2a shows that most of the events in study are located within a focal depth range 0–10 km, thus leading to $r_u = 10$ km. Clearly, for the 3D measure r_u is much shorter than r_c and mainly controlled by the focal depth of 10 km within which most of the events are located. Figure 2a displays that there are several tens of events with 10 km $\leq H \leq 25$ km. The depth range $10 - 25$ km is longer than that $0 - 10$ km. Hence, the spatial structure of the hypocentral distribution for the 3D measure is very sparse because there are many voids within the structure, especially in the depth range $10 - 25$ km. This makes the log–log plots of $C_q(r)$ versus r be very scattering, especially for $\log(r) > 1.0$, thus being unable to lead to a wide enough range of $\log(r)$ for the linear pattern of data points. Hence, we cannot estimate the value of D_q for the 3D measure.

Wang and Lin (1993) and Wang and Lee (1996) measured the multifractal dimensions for the earthquakes with $M_D \geq 1$ ($M_D =$ the duration magnitude) in west Taiwan. They divided the study area into the north and south zone. They obtained that all D_q's are smaller than 2 and the values of D_q ($= 1.4$–1.6) in the south zone with $r_u = 40$ km are larger than those ($= 1.0$–1.3) in the north zone with $r_u = 25$ km. The values of $r_u = 40$ and 25 km are almost the smallest widths of epicentral distributions of the north and south zones, respectively. Considering 2D measure, the values of D_q of the 2021 Hualien earthquake swarm are smaller than those measured by Wang and Lee (1996) for earthquakes in the north and south zones in west Taiwan. The lower-bound magnitude was 1 for the earthquakes used by Wang and Lee (1996) and is 3 for the events of this study. This suggests that when more events with smaller magnitudes are taken into account, the values of D_q should be larger because of a decrease in spatial voids. For both 2D and 3D measures, Wang et al. (2014) measured the values of D_q from the $M_L \geq 3$ shallow earthquakes with $H \leq 40$ km in the Taipei Metropolitan Area (TMA) during 1973–2010. In their study, the linear portion of the log–log plot of $C_q(r)$ versus r appears in between $\log(r_l)$ and $\log(r_u)$. For the 2D and 3D measures, the value of $\log(r_l)$ is 0.3 that is similar to the value of this study. The values of $\log(r_u)$ are 1.7 and 1.4, respectively, for the 2D and 3D measures. For the 2D measure, their value is larger than that of this study. Their values of D_q are smaller than the spatial dimensions 2 and 3, respectively, for the 2D and 3D measures. Their values of D_q for 2D measures are similar to those of this study, thus suggesting similar 2D fractal structures in the two areas.

5.2 Time sequence of earthquakes

For the time sequence, the log–log plots of $C_q(t)$ versus t as displayed in Fig. 6 for $0.5 \leq \log(t) \leq 2.15$. Clearly, the log–log plot shows a linear relationship in a large range of $0.5 \leq \log(t) \leq 1.0$ in which the value of D_q are evaluated. This suggests that the time sequence of $M_L \geq 3$ earthquakes of the swarm is multifractal. The values of D_q are all smaller than 0.475 and much smaller than 1. Table 1 and Fig. 5 with solid squares exhibit that as $q > 10$, the values of D_q are very similar for different q's. The upper bound time for the linear portion is $\log(t_u) = 1.0$ or $t_u = 10$ days. This value is only slightly larger than the maximum inter-event time of 8.792 days of the time sequence. This suggests that the maximum inter-event time is a factor in controlling whether or not a time sequence is multifractal.

Kagan and Jackson (1991) stated that the 1D process is Poissonian if the correlation dimension (i.e., D_2) is 1, that is the standard time dimension, over the whole time period from zero to infinity. For global seismicity, they found that the mainshocks of earthquake sequences are specified with long-term, weak clustering and governed by a power-law temporal distribution. The correlation dimension of time sequences of those mainshocks is 0.8–0.9. This suggests that the mainshock occurrence is almost a stationary Poisson process. Wang (1996) measured the values of D_q for 44 $M_s \geq 7$ earthquakes of Taiwan from 1900 to 1994 (Wang and Kuo 1995). Only the values of D_q for $q < 7$ were measured because the log–log plot of $C_q(t)$ versus t is linearly well distributed for q < 7. This indicates that $M_s \geq 7$ earthquakes in Taiwan shows multifractality only for the coarse structures of time sequence. In addition, the earthquake sequence shows a somewhat strong Poisson process because of $D_2 = 0.72$. Smalley et al. (1987) measured the values D_2 for the seismicity of the New Hebrides between mid-1978 and mid-1984. The measured values are $D_2 = 0.126$–0.255. This makes them to assume that the earthquake occurrences significantly deviate from random or Poisson behavior. In comparison with previous three studies, the component

Wang *et al. Terrestrial, Atmospheric and Oceanic Sciences*   (2022) 33:11

Page 8 of 9

of Poisson processes is weak in the time sequence of the 2021 Hualien earthquake swarm because of $D_2 = 0.475$.

6 Conclusions

An earthquake swarm occurred in the Hualien area (from 23°47′ N to 24°04′ N and from 121°25′ E to 121°42′ E) during April 7–August 31, 2021. From the $M_L \geq 3$ events with $H \leq 25$ km, the values of $C_q(r)$ are calculated for the spatial distributions of both epicenters (2D measure) and hypocenters (3D measure) based on the distance between two events, r, and those of $C_q(t)$ for the time sequence using the inter-event time between two events, t. The values of D_q are measured from the linear portions of the log–log plots of $C_q(r)$ versus r and $C_q(t)$ versus t. In the space domain, the maximum epicentral and hypocentral distance are 42.29 km and 49.12 km, respectively. The degree of scattering of data points is much higher for the 3D measure than for the 2D measure. For the 2D measure, there is a linear pattern in the range $\log(r_o) \leq \log(r) \leq \log(r_u)$ and roll-over when $\log(r) > \log(r_u)$ on the log–log plot. The values of $\log(r_o)$ and $\log(r_u)$ are, respectively, 0.5 and 1.3. The values of D_q are all smaller than 2 that is the spatial dimension in Euclidean geometry and monotonically decreases with increasing q. This indicates that the epicentral distribution of $M_L \geq 3$ earthquakes of the swarm shows multifractality when the epicentral distances are shorter than $r_u = 20.0$ km, which is shorter than the length of the study area along either the latitude or the longitude. On the other hand, there is only a narrow linear pattern of data points on the log–log plot under the 3D measure for the hypocentral distribution. This means that the hypocentral distribution of $M_L \geq 3$ earthquakes of the swarm is not multifractal. In the time domain, the maximum inter-event time is 8.792 days. The log–log plot of $C_q(t)$ versus t does show a linear pattern in a range of $0.5 \leq \log(t) \leq 1.0$, thus suggesting multifractality of the time sequence of $M_L \geq 3$ events of the swarm when the inter-event intervals are shorter than 8.792 days.

Author contributions
JHW carried out the calculations and drafted the manuscript. KCC checked up the earthquake data and plotted the spatial and depth distributions of epicenters and time variations of events. KCC collected and provided the earthquake data. KHK deeply discussed the physical meaning of results and corrected numerous typo errors. All authors read and approved the final manuscript.

Author details
[1]Institute of Earth Sciences, Academia Sinica, Nangang, P.O. Box 1-55, Taipei, Taiwan. [2]Department of Earth Sciences, National Central University, Taoyuan, Taiwan. [3]Seismological Center, Central Weather Bureau, Taipei, Taiwan. [4]Department of Geological Sciences, Pusan National University, Busan, Republic of Korea.

References
Aviles CA, Scholz CH, Boatwright J (1987) Fractal analysis applied to characteristic segments of the San Andreas fault. J Geophys Res 92:331–344
Chang YF, Chen CC, Liang CY (2007) The fractal geometry of the surface ruptures of the 1999 Chi-Chi earthquake Taiwan. Geophys J Int 170:170–174
Chen KC, Wang JH (1986) The May 20, 1986 Haulien, Taiwan earthquake and its aftershocks. Bull Inst Earth Sci Acad Sin 6:1–13
Chen KC, Wang JH (1988) A study on aftershocks and focal mechanisms of two 1986 earthquakes in Hualien, Taiwan. Proc Geol Soc China 31:65–72
Chen HY, Kuo LC, Yu SB (2004) Coseismic movement and seismic ground motion associated with the 31 March 2002 off Hualien, Taiwan, earthquake. Terr Atmos Ocean Sci 15(4):683–695
Chen KH, Toda S, Rau RJ (2007) A leaping, triggered sequence along a segmented fault: the 1951 M_L 7.3 Hualien-Taitung earthquake sequence in eastern Taiwan. J Geophys Res 113:B02304. https://doi.org/10.1029/2007JB005048
Fan X, Lin M (2017) Multiscale multifractal detrended fluctuation analysis of earthquake magnitude series of Southern California. Physica A 479:225–235. https://doi.org/10.1016/j.physa.2017.03.003
Gotoh K, Hayakawa M, Smirnova N (2003) Fractal analysis of the ULF geomagnetic data obtained at Izu Peninsula, Japan in relation to the nearby earthquake swarm of June–August 2000. Nat Hazard Earth Sys Sci 3(3/4):229–236
Grassberger P (1983) Generalized dimensions of strange attractors. Phys Lett 97A:227–230
Grassberger P, Procaccia I (1983) Measuring the strangeness of strange attractors. Physica D 9:189–208
Gutenberg B, Richter CF (1944) Frequency of earthquakes in California. Bull Seism Soc Am 34:185–188
Hentschel HGE, Procaccia I (1983) The infinite number of generalized dimensions of fractals and strange attractors. Physica 8D:435–444
Hirabayashi T, Ito K, Yoshii T (1992) Multifractal analysis of earthquakes. Pure Appl Geophys 138:591–610
Hirata T (1989) A correlation between the *b* value and the fractal dimension of earthquakes. J Geophys Res 94:7507–7514
Hsu MT (1961) Seismicity of Taiwan (Formosa). Bull Earthquake Res Inst Tokyo Univ 39:831–847
Hsu MT (1971) Seismicity of Taiwan and some related problem. Bull Int Inst Seism Earthquake Engin Japan 8:41–160
Hui C, Cheng C, Ning L, Yang J (2020) Multifractal characteristics of seismogenic systems and *b* values in the Taiwan seismic region. Int J Geo-Inf 9:384. https://doi.org/10.3390/ijgi9060384
Hwang RD, Lin CY, Chang WY, Lin TW, Huang YL, Chang JP (2019) Multiple-event analysis of the 2018 M_L 6.2 Hualien earthquake using source time functions. Terr Atmos Ocean Sci 30(3):367–376
Ida Y, Yang D, Li Q, Sun H, Hayakawa M (2012) Fractal analysis of ULF electromagnetic emissions in possible association with earthquakes in China. Nonlin Processes Geophys 19:577–583. https://doi.org/10.5194/npg-19-577-2012
Kagan YY, Jackson DD (1991) Long-term earthquake clustering. Geophys J Int 104:117–133
Karney CFF (2012) Algorithms for geodesics. http://geographiclib.sourceforge.net/geod.html
Kim KH, Chiu JM, Pujol J, Chen KC, Huang BS, Yeh YH, Shen P (2005) Three-dimensional V_P and V_S structural models associated with the active

Wang *et al. Terrestrial, Atmospheric and Oceanic Sciences*   (2022) 33:11

Page 9 of 9

subduction and collision tectonics in the Taiwan region. Geophys J Int 162:204–220

Kiyashchenko D, Smirnova N, Troyan V, Saenger E, Vallianatos F (2004) Seismic hazard precursor evolution: fractal and multifractal aspects. Phys Chem Earth Parts a/b/c 29(4–9):367–378

Koyama J, Zang SX, Ouchi T (1995) Mathematical modeling and stochastic scaling of complex earthquake activity. In: Koyama, Feng (eds) Advance in mathematical seismology. Seismological Press, Beijing, pp 165–180

Kuo-Chen H, Guan Z, Sun W, Jhong P, Brown D (2019) Aftershock sequence of the 2018 Mw64 Hualien earthquake in eastern Taiwan from a dense seismic array data set. Seismol Res Lett 90(1):60–67

Kurths J, Herzel H (1987) An attractor in a solar time series. Physica 225:165–172

Lee HK (1995) Fractal clustering of fault activity in California. Geology 23:377–380

Lee YH, Chen GT, Rau RJ, Ching KE (2008) Coseismic displacement and tectonic implication of 1951 Longitudinal Valley earthquake sequence, eastern Taiwan. J Geophys Res 113:B04305. https://doi.org/10.1029/2007JB005180

Li D, Zheng Z, Wang B (1994) Research into the multifractal of earthquake spatial distribution. Tectonophys 233:91–97

Ma KF, Wang JH, Zhao D (1996) Three-dimensional seismic velocity structure of the crustal and uppermost mantle beneath Taiwan. J Phys Earth 44:85–105

Mandelbrot BB (1983) The fractal geometry of nature. W.H. Freeman, New York, p 468

Mandelbrot BB (1989) Multifractal measures, especially for the geophysicist. Pure Appl Geophys 131:5–42

Marquez-Ramirez VH, Alejandro F, Pichardo N, Reyes-Davila G (2012) Multifractality in seismicity spatial distributions: Significance and possible precursory applications as found for two cases in different tectonic environments. Pure Appl Geophys 169(12):2091–2105

Ni C, Zhang S, Chen Z, Yan Y, Li Y (2017) Mapping the spatial distribution and characteristics of lineaments using fractal and multifractal models: a case study from Northeastern Yunnan Province, China. Sci Rept 7:10511. https://doi.org/10.1038/s41598-017-11027-0

Ogata Y, Abe K (1991) Some statistical features of the long-term variation of the global and regional seismicactivity. Int Stat Rev 59:139–161

Okubo PG, Aki K (1987) Fractal geometry in the San Andreas fault system. J Geophys Res 92:345–355

Oncel AO, Main I, Alptekin O, Cowie P (1995) Spatial variations of the fractal properties of seismicity in the Anatolian fault zones. Tectonophysics 257:189–202

Papadopoulos GA, Dedousis V (1992) Fractal approach of the temporal earthquake distribution in the Hellenic arc-trench system. Pure Appl Geophys 139:269–276

Rau RJ, Wu FT (1995) Tomographic imaging of lithospheric structures under Taiwan. Earth Planet Sci Lett 133:517–532. https://doi.org/10.1016/0012-821X(95)00076-O

Shin TC (1992) Some implications of Taiwan tectonic features from the data collected by the Central Weather Bureau Seismic Network. Meteorol Bull CWB 38:23–48 (**in Chinese**)

Shin TC, Chang CH (2005) Taiwan's seismic observational system. In: Wang JH, Wang CY, Sung QC, Shin TC, Yu SB, Shieh CF, Wen KL, Chung SL, Lee M, Kuo KM, Chang KC, Chung SL (Eds.), *The 921 Chi-Chi Major Earthquake*, Office of Inter-Ministry S&T Program for Earthquake and Active-fault Research, NSC, pp. 60–82. (in Chinese)

Smalley RF Jr, Chatelan J-L, Turcotte DL, Prevot R (1987) A fractal approach to the clustering of earthquakes: applications to the seismicity of the New Hebrides. Bull Seism Soc Am 77:1368–1381

Smirnova NA, Kiyashchenko DA, Troyan VN, Hayakawa M (2012) Multifractal approach to study the earthquake precursory signatures using the ground-based observations. Rev Appl Phys 2(3):58–67

Sri Lakshmi S, Banerjee P (2019) Dynamic multifractality of seismic activity in Northeast India. Pure Appl Geophys 176(6):1561–1577. https://doi.org/10.1007/s00024-018-02087-y

Takayasu H (1990) Fractals in the physical sciences. Manchester Univ. Press, Manchester

Tang YJ, Chang YF, Liou TS, Chen CC, Wu YM (2012) Evolution of the temporal multifractal scaling properties of the Chiayi earthquake (M_L=6.4) Taiwan. Tectonophys 546–547:1–9

Telesca L, Cuomo V, Lapenna V, Macchiato M (2001) Identifying space–time clustering properties of the 1983–1997 Irpinia-Basilicata (Southern Italy) seismicity. Tectonophysics 330:93–102

Tsai YB, Teng TL, Chiu JM, Liu HL (1977) Tectonic implications of the seismicity in the Taiwan region. Mem Geol Soc China 2:13–41

Turcotte DL (1989) Fractal in geology and geophysics. Pure Appl Geophys 131:171–196

Wang JH (1988a) *b* values of shallow earthquakes in Taiwan. Bull Seism Soc Am 78:1243–1254

Wang JH (1988b) Temporal change of duration ratios for foreshocks and aftershocks of a moderate Taiwan earthquake. Proc Geol Soc China 31:99–110

Wang JH (1989) The Taiwan telemetered seismographic network. Phys Earth Planet Inter 58:9–18

Wang JH (1996) Multifractal measures of time series of $M{\geq}7$ earthquakes in Taiwan. J Geol Soc China 39:117–123

Wang JH (1998) Studies of earthquake seismology in Taiwan during the 1897–1996 period. J Geol Soc China 41:291–336

Wang JH (2018) A review on scaling of earthquake faults. Terr Atmos Ocean Sci 29(6):589–610

Wang JH (2019) A review on scaling of source spectra. Surv Geophys 41(2):133–166. https://doi.org/10.1007/s10712-019-09512-4

Wang JH, Kuo HC (1995) A catalogue of $M{\geq}7$ Taiwan earthquakes (1900–1994). J Geol Soc China 38:95–106

Wang JH, Lee CW (1995) Multifractal characterization of an earthquake sequence. Physica A 221:152–158

Wang JH, Lee CW (1996) Multifractal measures of earthquakes in west Taiwan. Pure Appl Geophys 146:131–145

Wang JH, Lin WH (1993) A fractal analysis of earthquakes in west Taiwan. Terr Atmos Ocean Sci 4:457–462

Wang JH, Shen HY (1999) Multifractal measures of epicentral distribution of $M{\geq}6$ earthquakes in the north-south seismic belt of Mainland China. J Geol Soc China 42:631–637

Wang CY, Shin TC (1998) Illustrating 100 years of Taiwan seismicity. Terr Atmos Ocean Sci 9:589–614

Wang JH, Tsai YB, Chen KC (1983) Some aspects of seismicity in Taiwan region. Bull Inst Earth Sci Acad Sin 3:87–104

Wang JH, Chen KC, Lee TQ (1994) Depth distribution of shallow earthquakes in Taiwan. J Geol Soc China 37:125–142

Wang JH, Chen KC, Huang WG, Chang KH, Wang JC, Leu PL (2014) Multifractal measures of $M{\geq}3$ shallow earthquakes in the Taipei Metropolitan Area. Terr Atmos Ocean Sci 25(1):19–28. https://doi.org/10.3319/TAO.2013.09.09.01(T)

Wen YY, Wen S, Lee YH, Ching KE (2019) The kinematic source analysis for 2018 M_w6.4 Hualien, Taiwan earthquake. Terr Atmos Ocean Sci. 30(3):377–387

Wu FT (1978) Recent tectonics of Taiwan. J Phys Earth 2(Suppl):S265–S299

Yeh YL, Wang JH, Chen KC (1990) Temporal-spatial source function of the May 20, 1986 Hualien, Taiwan Earthquake. Proc Geol Soc China 33:109–126

Yu SB, Chen HY, Kuo LC, Lallemand SE, Tsien HH (1997) Velocity field of GPS stations in the Taiwan area. Tectonophys 274:41–59

Zhao J, Chen S, Zuo R, Carranza E (2011) Mapping complexity of spatial distribution of faults using fractal and multifractal models: vectoring towards exploration targets. Comput Geosci 37(12):1958–1966

Publisher's note